Binuclear 1,2,4,5-Tetraimino-3,6-diketocyclohexane Bis[bis(Bipyridine)ruthenium(II)] Redox Series

Hitoshi Masui,[†,‡] Assunta L. Freda,[†] Michael C. Zerner,[§] and A. B. P. Lever*[,†]

Departments of Chemistry, York University, North York, Toronto, Ontario, Canada M3J 1P3, and University of Florida, Gainesville, Florida 32611

Received July 15, 1998

The reaction of the $[Ru(bpy)_2(MeOH)_2]^{2+}$ cation (bpy = 2,2′-bipyridine) with 1,2,4,5-tetraaminobenzene in the presence of trace water and oxygen yields the cation $[(bpy)_2Ru(1,2,4,5\text{-tetraimino-3,5-diketocyclohexane})Ru(bpy)_2]^{4+}$. This binuclear species undergoes ligand-based reductions, giving the 3+ and 2+ charged species. The X-ray structure, electrochemistry, ZINDO calculations, and NMR, ESR, UV/vis, and IR spectra were analyzed where possible, giving an electronic model of the binuclear species and some of its redox products. The X-ray structure reveals the $[(bpy)_2Ru]$ fragments symmetrically disposed across the 1,2,4,5-tetraimino-3,5-diketocyclohexane bridge in a molecule with C_s symmetry.

A. Introduction

We have recently been concerned[1−14] with the electronic properties of the ruthenium complexes of the noninnocent quinonoid systems with (O,O), (NH,O), (NH,NH), and recently (NH,S)[15] coordinating atoms. Our interest has lain with studies of the extent of coupling between metal dπ and ligand π and π* levels as a function of the net oxidation state of the system. It is evident that this coupling is very strong but can be controlled by changes in oxidation state. Thus, these species are candidates for molecular switches,[11,16−20] prompting us to study binuclear and ultimately oligonuclear fragments.[10−12]

Low-lying π*-orbitals of these ligands appear to mix extensively with the valence d-orbitals of the metal, giving complexes with essentially covalent frontier orbitals (HOMO and LUMO).[2,9,13] Thus, subject to symmetry constraints, the valence π-electrons become delocalized over both metal and ligand.

We anticipated that if a quinonoid ligand were used to bridge two ruthenium centers, a pronounced delocalization over the bridge and the two metal centers would result. Such a delocalization apparently occurs in the *p*-benzoquinonediimine-bridged complex $[(NH_3)_5Ru\text{-}p\text{-}BQDI\text{-}Ru(NH_3)_5]$[21−23] and in other bridged systems such as the 3,6-bis(2-pyridyl)-1,2,4,5-tetrazine (bptz) species[24] and various terpyridine systems[25] and is, of course, well-known in the Creutz−Taube ion and related species.[26,27] Recently some bridged tetraoxobenzene and -naphthalene analogues of the molecule under study here have also appeared.[28−32] Coupling through a *p*-quinone-bridged diruthenium and diosmium species is also relevant.[33]

Further, if such a bridge were used to link ruthenium centers in a linear polymeric chain, valence and conduction bands may develop, leading to semiconducting or conducting polymers required for molecular electronic devices. Such band develop-

† York University.
‡ Current address: Department of Chemistry, Kent State University, Kent, OH 44242.
§ University of Florida.

(1) Delmedico, A.; Fielder, S. S.; Lever, A. B. P.; Pietro, W. J. *Inorg. Chem.* **1995**, *34*, 1507.
(2) Masui, H.; Lever, A. B. P. *Inorg. Chem.* **1993**, *32*, 2199.
(3) Lever, A. B. P.; Auburn, P. R.; Dodsworth, E. S.; Haga, M. A.; Liu, W.; Melnik, M.; Nevin, W. A. *J. Am. Chem. Soc.* **1988**, *110*, 8076.
(4) Masui, H.; Lever, A. B. P.; Auburn, P. R. *Inorg. Chem.* **1991**, *30*, 2402.
(5) Haga, M.-A.; Lever, A. B. P.; Dodsworth, E. S. *J. Am. Chem. Soc.* **1986**, *108*, 7413.
(6) Haga, M. A.; Dodsworth, E. S.; Lever, A. B. P. *Inorg. Chem.* **1986**, *25*, 447.
(7) Auburn, P. R.; Dodsworth, E. S.; Haga, M.; Liu, W.; Nevin, W. A.; Lever, A. B. P. *Inorg. Chem.* **1991**, *30*, 3502.
(8) Tse, Y. H.; Auburn, P. R.; Lever, A. B. P. *Can. J. Chem.* **1992**, *70*, 1849.
(9) Metcalfe, R. A.; Lever, A. B. P. *Inorg. Chem.* **1997**, *36*, 4762. Metcalfe, R. A.; Vasconcellos, L. C. G.; Mirza, H.; Franco, D. W.; Lever, A. B. P. *J. Chem. Soc., Dalton Trans.* **1999**, 2653.
(10) Metcalfe, R. A.; Dodsworth, E. S.; Fielder, S. S.; Stufkens, D. J.; Lever, A. B. P.; Pietro, W. J. *Inorg. Chem.* **1996**, *35*, 7741.
(11) Metcalfe, R. A.; Dodsworth, E. S.; Lever, A. B. P.; Pietro, W. J.; Stufkens, D. J. *Inorg. Chem.* **1993**, *32*, 3581.
(12) Delmedico, A.; Auburn, P. R.; Dodsworth, E. S.; Lever, A. B. P.; Pietro, W. J. *Inorg. Chem.* **1994**, *33*, 1583. Del Medico, A.; Pietro W. J.; Lever, A. B. P. *Inorg. Chim. Acta* **1998**, *281/2*, 126.
(13) (a) Masui, H.; Lever, A. B. P.; Dodsworth, E. S. *Inorg. Chem.* **1993**, *32*, 258. (b) Masui, H. Ph.D. Dissertation, York University, Toronto, Ontario, Canada, 1994; p 158. (c) Masui, H.; Lever, A. B. P. Unpublished observations.
(14) Cunha, C. J.; Dodsworth, E. S.; Lever, A. B. P. *Inorg. Chim. Acta* **1996**, *242*, 293.
(15) Ebadi, M.; Lever, A. B. P. *Inorg. Chem.* **1999**, *38*, 467.
(16) Joulie, L. F.; Schatz, E.; Ward, M. D.; Weber, F.; Yellowlees, L. J. *J. Chem. Soc., Dalton Trans.* **1994**, 799.
(17) Ward, M. D. *Chem. Soc. Rev.* **1995**, *24*, 121.
(18) Wlodarczyk, A.; Maher, J. P.; Mccleverty, J. A.; Ward, M. D. *J. Chem. Soc., Chem. Commun.* **1995**, 2397.
(19) Bolger, J.; Gourdon, A.; Ishow, E.; Launay, J. P. *Inorg. Chem.* **1996**, *35*, 2937.
(20) Fees, J.; Kaim, W.; Moscherosch, M.; Matheis, W.; Klima, J.; Krejcik, M.; Zalis, S. *Inorg. Chem.* **1993**, *32*, 166.
(21) Joss, S.; Reust, H.; Ludi, A. *J. Am. Chem. Soc.* **1981**, *103*, 981.
(22) Joss, S.; Burgi, H. B.; Ludi, A. *Inorg. Chem.* **1985**, *24*, 949.
(23) Joss, S.; Hasselbach, K. M.; Bürgi, H. B.; Wordel, R.; Wagner, F. E.; Ludi, A. *Inorg. Chem.* **1989**, *28*, 1815.
(24) Johnson, J. E. B.; Degroff, C.; Ruminski, R. R. *Inorg. Chim. Acta* **1991**, *187*, 7380.
(25) Beley, M.; Collin, J.-P.; Louis, R.; Metz, B.; Sauvage, J.-P. *J. Am. Chem. Soc.* **1991**, *113*, 8521.
(26) Creutz, C. *Prog. Inorg. Chem.* **1983**, *30*, 1.
(27) Creutz, C. C.; Taube, H. *J. Am. Chem. Soc.* **1969**, *91*, 3988. Creutz, C. C.; Taube, H. *J. Am. Chem. Soc.* **1973**, *95*, 1086. Curtis, J. C.; Blackbourn, R. L.; Ennix, K. S.; Hu, S.; Roberts, J. A.; Hupp, J. T. *Inorg. Chem.* **1989**, *28*, 3791.

10.1021/ic980826q CCC: $19.00
Published on Web 12/18/1999

ment is observed in oligomers[34] of $(NH_3)_5Ru$-pyz-$\{(NH_3)_4Ru$-pyz-$\}_xRu(NH_3)_5$.

Our earlier studies on the electronic properties of substituted benzoquinone-diimine complexes[2,9−11,13] clearly pointed to the possibility of using 1,4-diamino-2,5-benzoquinonediimine as a bridging ligand of superior coordinating ability as compared to the monodentate *p*-benzoquinonediimine bridge. However, the bridge has two tautomeric forms, L-**1a** and L-**1b**, The *p*-diimine form, L-**1b**, having uninterrupted π-conjugation between the two metal centers, is expected to have greater communication between the metals than the *o*-diimine form, L-**1a**, in which the conjugation is broken by the amino groups. The *p*-diimine form is thus more likely to lead to polymers which can conduct along the chain. This latter form is then directly comparable to the tetraoxobenzene species and naphthalene species[28−32] and the chloranilic acid (3,6-dichloro-2,5-dihydroxy-1,4-benzoquinone) species.[35]

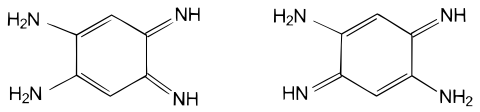

L-1a

L-1b

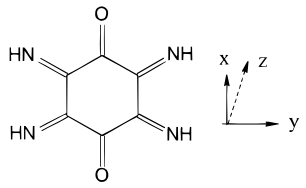

L-2

Attempts to synthesize the ruthenium bis(bipyridine) binuclear species of L-**1a** or L-**1b** gave, in high yield, a blue product which had many of the properties expected for the *p*-diimine tautomer. However, when the synthesis was modified to favor the formation of the binuclear species (i.e., rigorous deoxygenation and drying of reagents), the yield of the blue product declined and other products formed. The structure of a green oxidation product of the blue species was obtained, and it was found that the bridging ligand had been attacked by water, giving a bridged binuclear ruthenium(II) complex (**2**) of 1,2,4,5-tetraimino-3,6-diketocyclohexane, L-**2**. This is a nitrogen-containing analog of the hexaoxobenzenate anion (rhodizonate) whose bridged metal complexes have been known for a long time.[29−33,36,37] In this paper, we present the synthesis and characterization of **2** in its 4+ (**2**), 3+ (**3**), and 2+ (**4**) (net cationic charge) oxidation states and discuss the delocalization of the ruthenium d manifold through this bridge as a function of oxidation state. The 5+ and 6+ members of this series were also identified by electrochemistry but not further studied.

B. Experimental Section

B.1. Physical Methods. Cyclic voltammetry, spectroelectrochemistry, and coulometry were performed using Princeton Applied Research Corp. Models 173, 175, and 179 instrumentation. The working electrode was referenced to a AgCl/Ag/0.1 M Bu_4NPF_6/CH_3CN/glass frit reference electrode, whose potential was determined in a separate experiment versus the ferrocenium/ferrocene couple. All potentials are reported versus the standard calomel electrode (SCE), assuming $E_{1/2}$(ferrocenium/ferrocene) = 0.425 V vs SCE.[38] Spectroelectrochemistry was performed in a 1 cm glass cuvette with a perforated polyethylene cap through which a platinum mesh working electrode, a Nichrome counter electrode, and a AgCl/Ag reference electrode were inserted. The counter electrode was separated from the bulk solution by a glass frit. Solvent-saturated nitrogen gas was bubbled to stir the solution and provide an inert atmosphere.

Electronic spectra were obtained on a Hitachi-Perkin-Elmer Model 340 spectrometer. ^{1}H NMR spectra were obtained on a Bruker AM300 300 MHz or Bruker AMX 400 MHz spectrometer in d_3-acetonitrile. The electron paramagnetic resonance spectrum was obtained on a Varian E4, X-band spectrometer with the sample dissolved in frozen acetone solution and cooled to 100 K in a stream of cold nitrogen gas. The magnetic field was calibrated using 2,2-di(4-*tert*-octylphenyl)-1-picrylhydrazyl free radical standard, assuming $g = 2.0023$.

INDO/1 and INDO/S calculations used the ZINDO program and a Hyperchem platform (Hypercube, Waterloo, Ontario, v4.5 and later, 5.1). Data were processed on a Silicon Graphics Personal Iris Indigo R4000 or a Pentium 120 MHz Intel computer running ZINDO/1 geometry optimizations and ZINDO/S spectroscopic and molecular orbital calculations.[39−48] Interaction factors were $k_{p\sigma} = 1$ and 1.267 for ZINDO/1 and $k_{p\pi} = 1$ and 0.585 for ZINDO/S, together with the ruthenium bases of Krogh−Jespersen[49] but with Ru, $\beta(4d) = -20$ eV.[50] For the open shell 3+ species **3**, ROHF and CAHF data were derived using the developmental version of ZINDO running on an SGI Origin 2000 computer. See section C.6.3.2. for further details. Summary data concerning the geometries of the optimized structures are presented below (section C.1) and in more detail on our Web site as standard format Xmolxyz files.

(28) Dei, A.; Gatteschi, D.; Pardi, L. *Inorg. Chem.* **1990**, *29*, 1442. Bruni, S.; Cariati, F.; Dei, A.; Gatteschi, D. *Inorg. Chim. Acta* **1991**, *186*, 157.
(29) Ward, M. D. *Inorg. Chem.* **1996** *35*, 1712.
(30) Heinze, F.; Mann, S.; Huttner, G.; Zsolnai, L. *Chem. Ber.* **1996**, *129*, 1115.
(31) Dei, A.; Gatteschi, D.; Pardi, L.; Russo, U. *Inorg. Chem.* **1991**, *30*, 2589.
(32) Dei, A.; Gatteschi, D.; Pardi, L. *Inorg. Chim. Acta* **1991**, *189*, 125.
(33) Keyes, T. E.; Forster, R. J.; Jayaweera, P. M.; Coates, C. G.; McGarvey, J. J.; Vos, J. G. *Inorg. Chem.* **1998**, *37*, 5925.
(34) von Kameke, A.; Tom, G. M.; Taube, H. *Inorg. Chem.* **1978**, *17*, 1790.
(35) Calvo, M. A.; Lanfredi, A. M. M.; Oro, L. A.; Pinillos, M. T.; Tejel, C.; Tiripicchio, A.; Ugozzoli, F. *Inorg. Chem.* **1993**, *32*, 1147. Cueto, S.; Straumann, H. P.; Rys, P.; Petter, W.; Gramlich, V.; Rys, F. S. *Acta Crystallogr., Sect. C: Cryst. Struct. Commun.* **1992**, *48*, 458. Elduque, A.; Garces, Y.; Oro, L. A.; Pinillos, M. T.; Tiripicchio, A.; Ugozzoli, F. *J. Chem. Soc., Dalton Trans.* **1996**, 2155. Johnston, R. F.; Sengupta, P. K.; Ossain, M. B.; Vanderhelm, R.; Jeong, W. Y.; Holwerda, R. A. *Acta Crystallogr., Sect. C: Cryst. Struct. Commun.* **1990**, *46*, 1796. Tiripicchio. *Inorg. Chem.* **1993**, *32*, 1147. Zhang, M. X.; Liu, Z. L.; Yang, L.; Liu, Y. C. *J. Chem. Soc., Chem. Commun.* **1991**, 1054. Zubieta, J. *Chem. Commun.* **1988**, 1017.
(36) Pierpont, C. G.; Francesconi, L. C.; Hendrickson, D. N. *Inorg. Chem.* **1977**, *16*, 2367.
(37) Wrobleski, J. T.; Brown, D. B. *Inorg. Chem.* **1979**, *18*, 498.
(38) Lever, A. B. P. *Phthalocyanines: Properties and Applications;* VCH: New York, 1995; Vol. 3, p 3.
(39) Anderson, W. P.; Cundari, T.; Drago, R. S.; Zerner, M. C. *Inorg. Chem.* **1989**, *29*, 1.
(40) Anderson, W. P.; Cundari, T.; Zerner, M. C. *Int. J. Quantum Chem.* **1991**, *39*, 31. Anderson, W. P.; Edwards, W. D.; Zerner, M. C. *Inorg. Chem.* **1986**, *25*, 2728.
(41) Zerner, M. C. *Int. J. Quantum Chem.* **1989**, *35*, 567. Edwards, W. D.; Zerner, M. C. *Theor. Chim. Acta.* **1987**, *72*, 347.
(42) Martin, C.; Zerner, M. C. In *Inorganic Electronic Structure and Spectroscopy*; Lever, A. B. P.; Solomon, E. I., Eds.; J. Wiley and Sons: New York, 1999; Vol. 1, p 555.
(43) Bacon, A. D.; Zerner, M. C. *Theor. Chim. Acta* **1979**, *53*, 21.
(44) Zerner, M. C. *Metal−Ligand Interactions*; Kluwer Academic Publishers: Dordrecht, The Netherlands, 1996; p 493.
(45) Zerner, M. C.; Loew, G. H.; Kirchner, R. F.; Mueller-Westerhoff, U. T. *J. Am. Chem. Soc.* **1980**, *102*, 589.
(46) Culberson, J. C.; Knappe, P.; Rösch, N.; Zerner, M. C. *Theor. Chim. Acta* **1987**, *71*, 21.
(47) Ridley, J.; Zerner, M. C. *Theor. Chim. Acta* **1973**, *32*, 111.
(48) Ridley, J.; Zerner, M. C. *Theor. Chim. Acta* **1976**, *42*, 223.
(49) Krogh Jespersen, K.; Westbrook, J. D.; Potenza, J. A.; Schugar, H. J. *J. Am. Chem. Soc.* **1987**, *109*, 7025.
(50) Gorelsky, S. I.; Lever, A. B. P. Unpublished observations.

B.2. Preparation of [(bpy)$_2$Ru(C$_6$H$_4$N$_4$O$_2$)Ru(bpy)$_2$](ClO$_4$)$_4$·4H$_2$O (2). To a suspension of Ru(bpy)$_2$Cl$_2$ (0.100 g, 0.206 mmol)[51] in methanol (5 mL) was added silver nitrate crystals (0.0696 g, 0.409 mmol). The mixture was stirred for 2 h in air, during which time a red mixture formed. The mixture was filtered through Celite to remove AgCl. The filtrate was deoxygenated under a nitrogen atmosphere and cooled in an ice bath.

Degassed solutions of 10% Et$_3$N−methanol (0.0572 mL, 0.413 mmol) and 1,2,4,5-tetraaminobenzene hydrochloride (0.0293 g, 0.103 mmol) in 5 mL of methanol were prepared. The Et$_3$N−methanol solution was transferred via cannula to the suspension of 1,2,4,5-tetraaminobenzene hydrochloride in methanol. Upon formation of the free base the suspension became a translucent pink solution. The free base was then transferred to the solution of [Ru(bpy)$_2$(MeOH)$_2$]$^{2+}$ via cannula and the mixture allowed to reflux for 5 h, giving a purple solution.

After being cooled to room temperature, the mixture was diluted with 100 mL of methanol and was vigorously stirred in an atmosphere of oxygen for 30 min, yielding a blue or purple color. The mixture was filtered, and a solution containing NH_4PF_6 (0.08 g) in water (5 mL) was added to the filtrate. The solution was flash evaporated to a volume of 5 mL. The resulting precipitate was filtered, rinsed with cold water, and air-dried.

The crude product was dissolved in a minimal of acetone, and aqueous 1 M HCl was added, causing the product to precipitate as the chloride salt, which was isolated by centrifugation and redissolved in a minimum amount of aqueous 1 M HCl. The product was preferentially precipitated by adding acetone (5−10 mL), and isolated by centrifugation. The amount of acetone used depends on the amount of impurities present. The impurities are red, purple-red, or blue, while the product is green. The process of redissolving and reprecipitating the product was repeated until the dissolved product was bright green.

The hexafluorophosphate salt of the binuclear species **2** was obtained by dissolving the chloride salt in a minimum amount of aqueous 1 M HCl and adding a 10% stoichiometric excess of NH_4PF_6 dissolved in an equal volume of water. The mixture was allowed to sit for at least 24 h for complete precipitation. For X-ray diffraction quality crystals, two aqueous solutions, one containing 1 mM chloride salt and 1 M HCl, and another containing 0.1 M $NaClO_4$, were allowed to slowly diffuse together through a Nylon Millipore filter barrier. Bronze, rectangular plates formed on the filter. The yield varied from about 10% to 90%. Anal. Calcd for 4+ species (**2**), **2**(ClO$_4$)$_4$·4H$_2$O/C$_{46}$H$_{44}$Cl$_4$N$_{12}$O$_{22}$Ru$_2$: C, 37.81; H, 3.04; N, 11.50. Found: C, 36.54; H, 3.04; N, 11.19. NMR (with assignments) in d_3-acetonitrile for **2**(PF$_6$)$_4$: δ 7.51 (d, 4H, H6′); 7.54 (t, 4H, H5′); 7.62 (t, 4H, H5); 7.695 (d, 4H, H6); 8.17 (td, 4H, H4′); 8.27 (t, 4H, H4); 8.56 (d, 8H, H3, H3′); 13.65 (s, ═NH). There are also three signals (7.82 (t), 8.49 (d), 9.30 (d)) which integrate for about 15% of the main species and which may arise from the second isomer; see the comments at the end of this section and also the text.

Precipitation of **2** from a dilute NaOH/MeOH solution, yields the 3+ species (**3**). Anal. Calcd for 3+ species, **3**(PF$_6$)$_3$·4H$_2$O/C$_{46}$H$_{44}$F$_{18}$N$_{12}$O$_6$P$_3$Ru$_2$: C, 36.88; H, 2.96; N, 11.22. Found: C, 36.51; H, 2.89; N, 11.23.

The 2+ binuclear species (**4**) was produced by a Hg-pool bulk reduction of **2**(ClO$_4$)$_4$·4H$_2$O in deuterated acetonitrile with 0.1 M $NaClO_4$. A modified electrochemical cell with a Ag quasi-reference electrode and Ni−Cr wire counter electrode was used. The NMR spectrum of the oxygen-sensitive doubly reduced species in d_3-acetonitrile:

Assignments are given with the labels A and B to designate the two isomers (see the text); δ 7.18 (m, 4H, H5A′ + H5B′); 7.53, 7.54 (2t, 4H, H5B, H5A); 7.64, 7.65 (2d, 4H, H6B′, H6A′); 7.83 (t, 4H, H4A′ + H4B′); 8.01, 8.03 (q, 4H, H4A, H4B); 8.17 (br, 4H, ═NH); 8.32 (d, 4H, H3A + H3B); 8.39, 8.41 (2d, 4H, H3A′, H3B′); 8.49, 8.52 (2d, 4H, H6B, H6A). The apparent quartet at 8.01 and 8.03 is actually two overlapping triplets from separate species. Isomer A is the majority isomer, presumed to be of C_{2h} symmetry. The bipyridine ring protons are numbered conventionally from the bridgehead, the N atoms being at positions 2 and 2′. The primed protons reside on the pyridine ring trans to the bridging ligand. The notation H5A′ + H5B′ signifies overlapping signals while H5A′, H5B′ would signify distinct signals.

Table 1. Crystallographic Data for [(bpy)$_2$Ru{Didi}Ru(bpy)$_2$]$^{4+}$

empirical formula	$C_{46}H_{42}Cl_4N_{12}O_{21}Ru_2$	*V*, Å^3	1371.1(5)
fw	1442.86	*Z*	1
cryst syst, space group	triclinic, *P*-1	temperature, K	293(2)
a, Å	8.484(2)	wavelength, Å	0.71073
b, Å	10.910(2)	ρ_c, Mg m^{-3}	1.747
c, Å	16.026(3)	R1[a] (%)	4.96
α, deg	105.17(3)	wR2[b] (%)	12.64
β, deg	99.62(3)	R1[a] (%, all data)	6.55
γ, deg	100.51(3)	WR2[b] (%, all data)	13.81

[a] $R1 = \sum(|F_o| - |F_c|)/\sum|F_o|$. [b] $wR2 = 100\{\sum[w(F_o^2 - F_c2)^2]/\sum[w(F_o^2)^2]\}^{1/2}$ and $w = 1/[s^2(F_o^2) + (0.0807P)^2 + 1.1919P]$ where $P = (F_o^2 + 2F_c^2)/3$.

Table 2. X-ray Structure Bond Lengths[a] (Å) of [{Ru(bpy)$_2$}$_2$(tetraiminodiketo cyclohexane)](ClO$_4$)$_4$·4H$_2$O

Ru1−N6A	1.990(5)	Ru1−N4A	2.063(5)
Ru1−N5A	2.016(4)	Ru1−N3A	2.085(5)
Ru1−N1A	2.062(5)	Ru1−N2A	2.087(6)
C1−O1	1.209(7)	N3A−C30A	1.332(9)
C1−C2	1.481(8)	N3A−C34A	1.370(9)
C2−N6A	1.295(7)	C30A−C31A	1.387(10)
C2−C3	1.450(8)	C31A−C32A	1.352(13)
C3−N5A	1.287(7)	C32A−C33A	1.408(14)
N1A−C10A	1.335(9)	C33A−C34A	1.378(10)
N1A−C14A	1.362(8)	C34A−C44A	1.461(11)
C10A−C11A	1.372(9)	N4A−C40A	1.346(9)
C11A−C12A	1.368(11)	N4A−C44A	1.359(8)
C12A−C13A	1.370(12)	C40A−C41A	1.384(10)
C13A−C14A	1.382(10)	C41A−C42A	1.357(13)
C14A−C24A	1.470(10)	C42A−C43A	1.373(13)
N2A−C20A	1.328(9)	C43A−C44A	1.389(11)
N2A−C24A	1.361(8)	Cl1−O13	1.389(9)
C20A−C21A	1.381(11)	Cl1−O10	1.397(10)
C21A−C22A	1.358(13)	Cl1−O12	1.382(11)
C22A−C23A	1.371(13)	Cl1−O11	1.50(2)
C23A−C24A	1.367(11)		

[a] Data for disordered perchlorate are omitted.

B.3. Crystal Data and Data Collection. The Mo Kα (λ = 0.710 69 Å) X-ray diffraction data (Tables 1−3 and Figure 1) were collected from a crystal of the 4+ cation, **2**, with dimensions of 0.8 × 0.2 × 0.05 mm, using a Siemens *R*3*m*/v diffractometer and XSCANS v.2.B7e software. The cell parameters, a = 8.484(2) Å, b = 10.910(2) Å, c = 16.026(3) Å, α = 105.17(3)°, β = 99.62(3)°, γ = 100.51(3), were obtained from 45 independent reflections, while the intensity data for the structural solution was obtained from 3588 independent reflections in the range of 3.5° < Θ < 50°. No absorption corrections were applied. ψ scans were collected (524 data for 18 selected reflections) and parameters fitted to an ellipsoidal model (XEMP). Application to the full data set produced no significant improvement in *R*(INT) or the final *R* factor, and therefore no absorption correction was applied. The final analysis using the uncorrected intensities has *R*(INT) = 0.0357 leads to R1 = 0.0496 with no anomalies in thermal parameters or in the final difference map using 3588 unique data and 415 parameters with a GOOF = 1.078.

B.4. Solution and Refinement of Structure of the 4+ Cation, 2. The refinement was performed using the SHELXTL v.4.1 software and standard scattering factors.[52] A preliminary study suggested that a structural solution could be obtained in the triclinic space group *P*1 (noncentrosymmetric) or $P\bar{1}$ (centrosymmetric). Initially, the structure was solved in *P*1, using a Patterson map to locate the heavier atoms. A crude refinement was performed using difference Fourier maps and least-squares method on 2896 reflections having $F_o > 4\sigma(F_o)$. This revealed that the bipyridine ligands, perchlorate anions, and waters of crystallization were disposed about a center of symmetry located at

(51) Sullivan, B. P.; Salmon, D. J.; Meyer, T. J. *Inorg. Chem.* **1978**, *17*, 3334.

(52) *International Tables*; Internation Union of Crystallography; Vol. 4. pp 55, 99, 149.

Table 3. X-ray Structure Bond Angles (deg)[a] for [{Ru(bpy)$_2$}$_2$(tetraiminodiketocyclohexane)](ClO$_4$)$_4$·4H$_2$O

N6A−Ru1−N5A	77.0(2)	N1A−C14A−C24A	115.1(6)
N6A−Ru1 N1A	99.4(2)	C13A−C14A−C24A	124.7(6)
N5A−Ru1−N1A	89.5(2)	C20A−N2A−C24A	118.3(6)
N6A−Ru1−N4A	89.5(2)	C20A−N2A−Ru1	126.0(5)
N5A−Ru1−N4A	98.4(2)	C24A−N2A−Ru1	115.4(5)
N1A−Ru1−N4A	169.2(2)	N2A−C20A−C21A	121.6(8)
N6A−Ru1−N3A	94.1(2)	C22A−C21A−C20A	119.5(9)
N5A−Ru1−N3A	170.7(2)	C21A−C22A−C23A	119.9(8)
N1A−Ru1−N3A	94.5(2)	C24A−C23A−C22A	118.3(8)
N4A−Ru1−N3A	78.7(2)	N2A−C24A−C23A	122.4(8)
N6A−Ru1−N2A	176.4(2)	N2A−C24A−C14A	114.7(6)
N5A−Ru1−N2A	100.1(2)	C23A−C24A−C14A	122.9(7)
N1A−Ru1−N2A	78.3(2)	C30A−N3A−C34A	120.1(6)
N4A−Ru1−N2A	93.1(2)	C30A−N3A−Ru1	126.0(5)
N3A−Ru1−N2A	88.9(2)	C34A−N3A−Ru1	113.8(4)
O1−C1−C2	122.6(5)	N3A−C30A−C31A	122.1(8)
N6A−C2−C3	113.4(5)	C32A−C31A−C30A	117.9(9)
N6A−C2−C1	123.4(5)	C31A−C32A−C33A	121.6(8)
C3−C2−C1	123.1(5)	C34A−C33A−C32A	117.7(9)
N5A−C3−C2	114.2(5)	N3A−C34A−C33A	120.6(8)
C10A−N1A−C14A	118.3(6)	N3A−C34A−C44A	116.0(6)
C10A−N1A−Ru1	125.5(4)	C33A−C34A−C44A	123.4(7)
C14A−N1A−Ru1	116.2(5)	C40A−N4A−C44A	118.5(6)
N1A−C10A−C11A	123.6(7)	C40A−N4A−Ru1	125.6(4)
C12A−C11A−C10A	118.0(8)	C44A−N4A−Ru1	115.9(5)
C11A−C12A−C13A	119.7(7)	N4A−C40A−C41A	122.7(7)
C12A−C13A−C14A	120.1(7)	C42A−C41A−C40A	118.5(8)
N1A−C14A−C13A	120.2(8)	C41A−C42A−C43A	120.1(8)
C42A−C43A−C44A	119.7(8)	C43A−C44A−C34A	124.8(7)
N4A−C44A−C43A	120.5(7)	C3−N5A−Ru1	117.1(4)
N4A−C44A−C34A	114.7(6)	C2−N6A-Ru1	118.2(4)
O13−Cl1 O10	110.9(8)	O13−Cl1−O11	103.5(9)
O1−Cl1−O12	112.6(9)	O10−Cl1−O11	117.3(12)
O10−Cl1−O12	104.0(8)	O12−Cl1−O11	108.8(11)

[a] Data for disordered perchlorate are omitted.

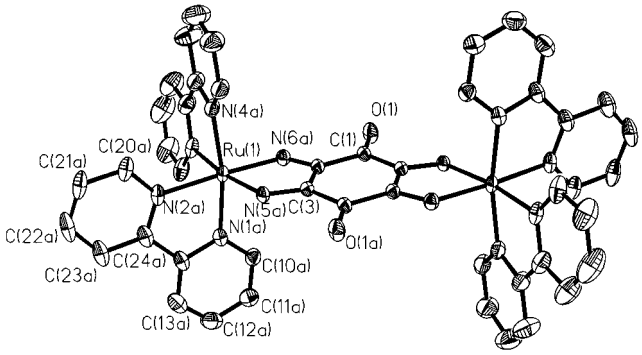

Figure 1. X-ray crystal structure of [{Ru(bpy)$_2$}$_2$(tetraiminodiketocyclohexane)](ClO$_4$)$_4$·4H$_2$O, drawn with 50% thermal ellipsoids. Only half of the atoms are labeled because of the centrosymmetry of the molecule.

the centroid of the binuclear species. Thus, the structure was resolved in $P\bar{1}$, using the previous positional parameters as a starting point for the refinement, and removing half of the atoms related by inversion. The hydrogen atoms were fixed at a distance of 0.96 Å for C−H bonds and 0.90 Å for N−H bonds, and were given fixed isotropic thermal parameters for the final refinement. The remaining atoms were given anisotropic thermal parameters for the final refinement. The perchlorate ions were constrained to have Cl−O bond lengths of 1.43 Å.[53] during the isotropic refinements but were constrained as a rigid group for the final anisotropic refinement. One of the perchlorates in the asymmetric unit was disordered by a 60° rotation about a Cl−O bond, and this was modeled by using six oxygen atoms with site occupation factors of 0.5. The refinement converged until the R index was 4.96% ($R = \sum||F_o| - |F_c||/\sum|F_o|$), and the largest difference Fourier peak and hole were 0.81 and −0.73 e/Å^3, respectively (around a perchlorate). Within the crystal the molecular symmetry is C_i, but it is close to C_{2h} and becomes C_{2h} following ZINDO/1 optimization with the C_2 axis containing the two ruthenium atoms. The local symmetry at the bridge is D_{2h} when the bipyridine rings are ignored.

C. Discussion

C.1. Molecular Structure (Tables 2 and 3 and Figure 1). The Ru−N, C−N, and C−C bond lengths within the metal−bridge chelate rings are similar to those of other coordinated primary α,α′-diimines (Table 2).[14,54] The short C−N bonds are significantly longer than that of a metal-free imine due to π-back-bonding into a π*-orbital that is antibonding with respect to the C−N bond.[55] The π*-orbital is also bonding with respect to the bridge metallocycle C−C bonds; thus, the C−C bond length is between those of a single bond and a double bond. The π-back-bonding also shortens the Ru−N bond such that the bridge has a shorter Ru−N bond than the bipyridines.

The intermediate bond orders of the Ru−N, C−N, and C−C bonds within the chelate ring can be likened to the intermediacy of bond orders within an aromatic ring.[56a] Indeed, there is a π-sextet counting the pair of π-back-bonding metal electrons. From this perspective, the coordinated bridging ligand is similar to anthraquinone. It is therefore not surprising that the structure of the bridge resembles the *p*-quinone fragment of anthraquinone.[56b]

Depending on the relative orientations of the bipyridine rings across the bridging ligand, there are in fact two possible diastereoisomers, the aforementioned C_{2h} and a second isomer of D_2 symmetry. As discussed in the NMR section below, evidence was obtained for this second isomer whose relative abundance varied from one preparation to another. We did not identify the experimental conditions which led to one isomer or the other, and as noted below, the electronic structural characteristics of the two isomers, as deduced from molecular computation, are very similar. The discussion in this paper therefore deals specifically with the C_{2h} isomer verified in the crystal structure.

C.2. Synthesis and Chemical Properties. The initial steps toward the formation of the bridging ligand probably consist of an aerial oxidation of the 1,2,4,5-tetraaminobenzene-bridged binuclear species to the 1,4-diamino-2,5-benzoquinonediimine-bridged binuclear species. This is followed by a 1,4-Michael addition of hydroxide on the 3- and 5-carbons. The final product results from the effective loss of eight hydrogen atoms. Since [Ru(bpy)$_2$(1,2-diamino-4,5-benzoquinonediimine)]$^{2+}$ is stable with respect to nucleophilic attack,[13] the presence of two coordinated Ru(bpy)$_2$ fragments probably makes the benzoquinonediimine bridge more susceptible to nucleophilic attack by withdrawing electron density from it.

Rigorous deoxygenation and dehydration of the reagents leads to a lower yield of **2**, presumably because oxygen is required for the initial oxidation step and water is required as a source of hydroxide. However, when the aerial oxidation is carried out in water, the main product is an unidentified navy-blue compound, believed[57] to be a hydrolyzed binuclear species. This

(53) Boglund, B.; Thomas, J. O.; Tellgren, R. *Acta Crystallogr., Sect. B* **1975**, *31*, 1842.

(54) Belser, P.; von Zelewsky, A.; Zehnder, M. *Inorg. Chem.* **1981**, *20*, 3089.

(55) Carugo, O.; Djinovic, K.; Rizzi, M.; Castellani, C. B. *J. Chem. Soc., Dalton Trans.* **1991**.

(56) (a) Carugo, O. *Inorg. Chim. Acta* **1994**, *215*, 219. (b) Prakash, A. *Acta Crystallogr.* **1967**, *22*, 439.

(57) The blue compound appears to have a high charge as it has a slightly lower R_f value than **2** on a TLC eluted with 1: 10 acetone/water containing 1% KNO$_3$. The blue species and **2** elute at similar rates on a gel exclusion column (Biobead SX1 eluted with 1:1 acetone/THF), indicating that they have similar molecular weights.

compound is one of the main contaminants in the synthesis of **2**. Reactions in which water and oxygen have been well removed lead to a red-brown compound after 24 h of reflux. This compound can also be produced by refluxing the $[Ru(bpy)_2$-(1,2-diamino-2,5-benzoquinonediimine)$]^{2+}$ monomer with[58] $[Ru(bpy)_2(MeOH)_2]^{2+}$, and appears to be a binuclear species—perhaps the sought orthodiimine binuclear species; these other products have not yet been characterized.

Species **2** is stable in 1 M HCl for many months and can be dissolved in concentrated H_2SO_4 to give a purple solution, which reverts to green when diluted with water. Above pH 8, the complex rapidly and irreversibly hydrolyzes to a red species, which then slowly converts to an orange-yellow decomposition product. In weakly basic methanol, the binuclear species **2** is in equilibrium with the one-electron-reduced species **3**.

C.3. NMR Spectra. The spectrum obtained for the 4+ cation, **2**, is fairly simple and easy to assign. The chemical shifts of the bipyridine protons are very similar to those observed[13b] in the species $[Ru(bpy)_2(bqdi)]^{2+}$. The NH protons resonate as a singlet at 13.65 ppm which is at lower field (higher δ) than any of the reported data for substituted bqdi complexes of $[Ru(bpy)_2]^{2+}$ and is significantly different from the data for the 2+ cation, **4** (8.17 ppm), described below. There appears to be only one dominant diastereoisomer in this spectrum. Three smaller signals *may* arise from the second isomer, whose other signals must then overlap the dominant species signals. The assignments were made in accordance with previous NMR analysis[13b] of $[Ru(bpy)_2(R\text{-}bqdi)]^{2+}$ species and of complexed bipyridines in general.[59] In this species, **2**, H3 and H3′ are coincident and at the lowest field of the aromatic protons. H6 and H6′ are both shifted upfield compared with the 2+ species, **4**, (see the Experimental Section and below), H6′ by about 0.1 ppm and H6 by about 0.8 ppm. The observed coupling constants are consistent with those in the literature.[59]

Species **4**, $Ru^{II}-(L^{2-})-Ru^{II}$, could in principle exist in the $S = 0$ ($\pi^*(1))^2$ or $S = 1$ ($\pi^*(1),\pi^*(2)$) configuration. The small difference in potential between the first and second reduction steps of the bridging ligand (see section C.4 below) suggests that the electrons may be entering two orbitals having significantly different spatial distributions, giving an $S = 1$ species. This would minimize the electronic repulsion between the electrons, and hence reduce the separation between the reduction potentials. The NMR spectrum of this electrochemically generated species, however, is sharp; i.e., it is neither broadened nor shifted by paramagnetism; the aromatic protons of the bipyridines appear in the region between 7 and 9 ppm. In fact, the species causes a slight diamagnetic upfield shift of the solvent peak (deuterated acetonitrile) as seen when the Evans method is employed.[60] For these reasons, the electronic configuration must be $S = 0$, but also see the comments below in section C.6.2.3.

For the 2+ cation, **4**, the most notable features of the proton NMR spectrum are the evident presence in the spectrum of two diastereoisomers and the deshielding of H6 (both diastereoisomers, A and B, see the Experimental Section). The deshielding can be explained by the 2-electron reduction of the bridge ligand which changes it from an 8-electron π-system to an aromatic 10-electron π-system with a significant ring current. The data are in fact very similar to those of the $[Ru(bpy)_2$(4,5-dimethoxy-1,2-diaminobenzene)$]^{2+}$ complex.[13a]

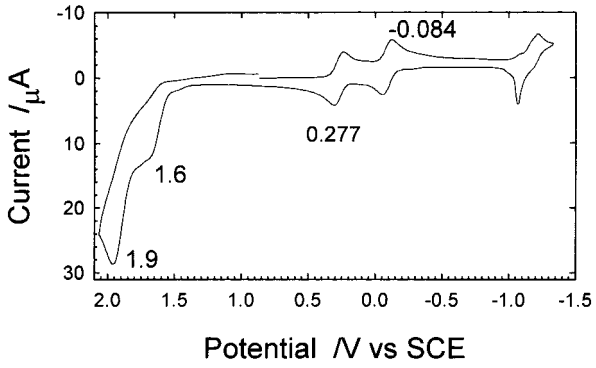

Figure 2. Cyclic voltammogram of $\{Ru(bpy)_2\}_2$(tetraiminodiketocyclohexane)$](ClO_4)_4$ (ca. 5 mM) at a Pt-disk electrode ($\phi = 0.5$ mm), in CH_3CN containing 0.3 M Bu_4NPF_6. The potentials are referenced to SCE.

The spectrum can readily be analyzed in terms of the existence of both diastereoisomers as indicated in the Experimental Section. The NMR data of diastereoisomers of dinuclear species have been previously reported by Keene and coworkers.[59a] Indeed they, in fact, separated them.

The NMR spectrum shows nine groups of signals in the aromatic region consistent with the eight inequivalent protons of bipyridine and the N−H of the bridging ligand. Each pyridine ring of bipyridine is expected to give rise, grossly, to two doublets (H3 and H6) and two triplets (H4 and H5). Further splitting by the para protons may give doublets of doublets and triplets of doublets. In the spectrum of the 2+ cation, **4**, it is clear that each of the signals around 7.6 and 8.5 ppm consists of a pair of doublets of different intensities, too close to integrate separately but, in this spectrum, in an approximate 3:2 ratio. This is consistent with the presence of the two diastereoisomers, present in different amounts. The remainder of the spectrum is consistent with this interpretation.

The two possible isomers have C_{2h} (Λ, Δ) or D_2 ($\Delta\Delta$, $\Lambda\Lambda$) symmetry, and both have only one bipyridine environment. Since there are two ways of obtaining the D_2 isomer, it should be the majority isomer, but the X-ray structure of species **2** was of the C_{2h} isomer. The majority isomer is labeled A and the minority B. H6 and H6′ are more deshielded in A than in B, while the reverse appears to be true for the other protons where it is possible to distinguish them. H3 and H4′ are almost exactly coincident in A and B.

C.4. Electrochemistry and Controlled Potential Electrolysis. The cyclic voltammogram of **2** dissolved in acetonitrile (Figure 2) exhibits two reversible one-electron couples[61] at 0.28 and −0.08 V vs SCE. These are insufficiently negative to be attributed to bipyridine or ruthenium reduction processes, and optical and electron paramagnetic resonance data reported below confirm they are bridge localized.

Controlled potential reduction in acetonitrile, just negative of the two reduction potential steps noted above, yields the 3+ and 2+ bridge reduced species as stable entities whose spectroscopic properties can be studied. Given the identity of the first two reduction processes as bridging ligand localized, with confirmatory data presented below, the 3+ species, **3**, is formally $Ru^{II}-(L^{-})-Ru^{II}$ and the 2+ species, **4**, is $Ru^{II}-(L^{2-})-Ru^{II}$. Species **4** was not isolated, but its optical spectrum,

(58) This compound is produced by reacting $Ru(bpy)_2Cl_2$ with $AgNO_3$ and is probably in equilibrium with $[Ru(bpy)_2(MeOH)_{2-n}(OMe)_n]^{n+}$.

(59) (a) Kelso, L. S.; Reitsma, D. A.; Keene, F. R. *Inorg. Chem.* **1996**, *35*, 5144. (b) Bolger, J. A.; Ferguson, G.; James, J. P.; Long, C.; McArdle, P.; Vos, J. G. *J. Chem. Soc., Dalton Trans.* **1993**, 1577. (c) Orelllana, G.; Ibarra, C. A.; Santoro, J. *Inorg. Chem.* **1988**, *27*, 1025. Constable, E. C.; Lewis, J. *Inorg. Chim. Acta* **1983**, *70*, 251.

(60) Evans, D. *J. Chem. Soc.* **1959**, 2003.

(61) One-electron processes were determined by coulometry.

Table 4. Observed and Calculated Electronic Spectral Data and Assignments for $[\{Ru(bpy)_2\}_2(tetraiminodiketocyclohexane)]^{n+}$, Redox Series[a]

species	obsd[b] (cm^{-1})	calcd[c] (cm^{-1})	assignment[d]
			HOMO = 152
4+	15 950 (4.47)	17 100 {0.63}	[151 → 153]$d\pi^+ - \pi$(bpy), π(bridge) → π^*(bridge) − $d\pi^-$, $^1B_{2u} \leftarrow {}^1A_{1g}$
	21 350 (4.27)	22 950 {0.53}	[149 → 154] $d\delta^- - \pi$(bpy), π(bridge) → π^*(bridge) − $d\delta^+$, $^1B_{2u} \leftarrow {}^1A_{1g}$
			[146 →153] π(bpy) → π^*(bridge) − $d\pi^-$, $^1B_{2u} \leftarrow {}^1A_{1g}$
	26 300 (4.06)	23 670 {0.35}	[149 → 154] $d\delta^- - \pi$(bpy), π(bridge) → π^*(bridge) − $d\delta^+$, $^1B_{2u} \leftarrow {}^1A_{1g}$
		26 620 {0.09}	[146 → 153] π(bpy) → π^*(1)(bridge), $^1B_{2u} \leftarrow {}^1A_{1g}$
		26 950 {0.05}	[149 → 155] [147 → 154] $^1B_{3u} \leftarrow {}^1A_{1g}$, d → π^*(2,3)(bridge)
	27 230 {0.22}		[152 → 155] [150 → 153] $^1B_{1u} \leftarrow {}^1A_{1g}$
			[149 → 155][147 → 154] $^1B_{3u} \leftarrow {}^1A_{1g,}$ d → π^*(2,3)(bridge)
	29 500sh	28 030 {0.13}	[152 → 157] [150 → 156] d → π^*(1)(bpy)
		28 310 {0.08}	[152 → 159] [150 → 158] d → π^*(1)(bpy)
		29 190 {0.20}	[149 → 157] [148 → 156] d → π^*(1)(bpy)
		30 560 {0.09}	[149 → 159] [148 → 158] d → π^*(1)(bpy)
		31 525 {0.19}	[151→ 158] [147→ 159] d → π^*(1)(bpy)
		31 654 {0.18}	var.
	34 900 (4.84)	33 310 {0.46}	[151 → 156] d → π^*(bpy),
		33 720 {1.10}	var.
	40 000 (4.65)	37 210 {0.67}	[152 → 163] [150 → 162] d → π^*(2)(bpy)
		37 690 {0.20}	[152 → 161] [150 → 160] d → π^*(2)(bpy)
		38 610 {0.72}	[149 → 163] d → π^*(2)(bpy)
		39 240 {0.19}	[151→ 160] d → π^*(2)(bpy)
		etc.	
			SOMO = 153
3+	8 500 (3.79)	4330 (0.18)	[153 → 154] $^2B_{3g} \leftarrow {}^2B_{1u}$, $\pi^* \rightarrow \pi^*$
	9 350 (3.63)	7770 (0.07)	[153 → 155] $^2B_{2g} \leftarrow {}^2B_{1u}$ $\pi^* \rightarrow \pi^*$
	12 350 (4.66)	11 350 (0.2)	[148 → 153] $^2B_{3g} \leftarrow {}^2B_{1u}$, $d_{yz} + \pi^* \rightarrow \pi^* - d_{yz}$
	17 350 (4.24)	16 400 (0.01)	[150 → 154] d → π^* (bridge), $^2B_{2g}$ _ $^2B_{1u}$
	22 400 (4.09)	20 100 (0.02)	[152 → 155] ... d → π^*(bridge), $^2B_{1g} \leftarrow {}^2B_{1u}$
		20 680 (0.04)	[153 → 158] π^* (bridge) + d → π^*(bpy)
		22 760 (0.44)	[147 → 154] ... $^2B_{3g} \leftarrow {}^2B_{1u}$
	24 050 (3.96)	24 000 (0.10)	Very mixed, d → π^* (bridge)
	etc.	24 770 (0.02)	Very mixed, d → π^* (bpy)
		26 780 (0.05)	Very mixed, d → π^* (bpy)
		26 870 (0.25)	
		etc.	
			HOMO = 153
2+	13 200 (4.32)	9 850 {0.15}	[153 → 155] d − π(bridge) → π^*(2)(bridge), $^1B_{3u} \leftarrow {}^1A_{1g}$
		11 400 {0.93}	[153 → 154] d − π(bridge) → π^*(3)(bridge), $^1B_{2u} \leftarrow {}^1A_{1g}$
	15 850sh (4.26)	15 600 {0.08}	[153 → 159] π^* (bridge) − $d\pi^- \rightarrow \pi^*$(1)(bpy)
	18 050 (4.46)	19 500 {0.55}	[152 → 155] $d\sigma^- \rightarrow \pi^*$(bridge), $^1A_{1u} \leftarrow {}^1A_{1g}$
	20 000sh	19 700 {0.21}	[152 → 159] [150 → 158] d → π^*(1)(bpy)
	etc. weak features	21 000 {0.35}	[151 → 157] [149 → 156] d → π^*(1)(bpy)
		23 100 {0.11}	[153 → 162] d → π^*(2)(bpy)
	26 100 (4.10)	24 500 {0.16}	many transitions, d, π(bridge) → π^*(2)(bpy)
		24 700 {0.09}	[147 → 154] $d\pi^- + \pi$(bridge) → π^*(bridge) − $d\pi^+$; [148 → 153] $d\pi^+ +$ π(bridge) → π^*(bridge) − $d\pi^-$
	28 900(4.06)	27 700 {0.04}	[147 → 155,159] [148 → 158] d + π(bridge) → π^*(1)(bpy), d → π^*(1)(bpy)
		28 100 {0.27}	[147 → 155] d + π(bridge) → π^*(2)(bridge), $^1B_{3u} \leftarrow {}^1A_{1g}$
		etc.	

[a] The electronic spectra were obtained spectroelectrochemically in CH_3CN containing 0.3 M Bu_4NPF_6. [b] Enclosed in the parentheses are log(molar absorbance, M^{-1} cm^{-1}) data. [c] Enclosed in braces are oscillator strength data. [d] Only the stronger predicted energies are listed here ($f \geq 0.01$). These energies are rather sensitive to the choice of β(4d)Ru.

obtained from spectroelectrochemical measurements, is discussed below.

There are two poorly resolved couples near the solvent limit at 1.6 V and 1.9 V (Figure 2), corresponding to formation of the 5+ and 6+ members of this redox series. A $\Delta E_{1/2}$ of about 0.3 V can be estimated from this pair of poorly resolved $Ru^{III/II}$ couples, indicating some degree of metal−metal communication, and a comproportionation constant of about 10^5 can be calculated for the reaction

$$4+ \text{ species} + 6+ \text{ species} \leftrightharpoons 2(5+ \text{ species})$$

The large oxidation currents at these couples are probably due to catalytic solvent oxidation, and cooling the cell significantly lowers the current. However, we were unable to fully resolve the couples.

C.5. Electron Paramagnetic Resonance. Reduction of the binuclear species **2** at 0.2 V gives species **3** with a 3+ charge[62] and a ligand-centered EPR signal (Figure S1), confirming bridging ligand localization of the unpaired electron, with the formal electronic configuration $Ru^{II}-(L^-)-Ru^{II}$.

The broadness and low g value of the EPR signal indicate significant delocalization of the unpaired electron over the ruthenium atoms,[63] consistent with the ZINDO calculations discussed below.

C.6. ZINDO Calculations and Electronic Spectra (Tables

(62) Microanalysis (Experimental Section) showed the presence of three $[PF_6]^-$ groups.

(63) Weil, J. A.; Bolton, J. R.; Wertz, J. E. *Electron Paramagnetic Resonance − Elementary Theory and Practical Applications*; John Wiley and Sons: New York, 1994. Ernst, S.; Hänel, P.; Jordanov, J.; Kaim, W.; Kasack, V.; Roth, E. *J. Am. Chem. Soc.* **1989**, *111*, 1733.

Table 5. Summary of Symmetries and Mixing and Splitting Energies[a]

orbital	$\Gamma(D_{2h})$	$\Gamma(C_{2h})$[b]	% Ru 4+ (**2**)	% Ru 3+ (**3**)	% Ru 2+ (**4**)
$xz + xz$ (δ)	b_{2g}	a_g	73	70	67
splitting, cm^{-1}			560	400	400
$xz - xz$ (δ)	a_u	a_u	76	71	66
$yz + yz$ (π)	b_{3g}	b_g	52	59	63
splitting, cm^{-1}			3220	1610	2010
$yz - yz$ (π)	b_{1u}	b_u	28	48	53
$x^2 - y^2 + x^2 - y^2$ (σ)	a_g	a_g	68	65	70
splitting, cm^{-1}			160	320	480
$x^2 - y^2 - x^2 - y^2$ (σ)	b_{2u}	a_u	69	66	71
π^* b_{1u}[c]	b_{1u}	b_u	37	18	17
π^* b_{2g}[c]	b_{2g}	a_g	3	2	1
π^* b_{3g}[c]	b_{3g}	b_g	25	12	8

[a] Raw data are shown in Tables 6−8. Due to round-off errors, sums in this table may not exactly agree with the appropriate sums in the other tables. [b] The required correlation involves the *y* axis in D_{2h} symmetry becoming the *z* axis in C_{2h} symmetry. For completion note that the $d\sigma^{*\pm}$ (dz^2) transforms as $a_g + b_{2u}$ in D_{2h} and $a_g + a_u$ in C_{2h} and $d\sigma^{*\pm}(d_{xy})$ as $b_{1g} + b_{3u}$ in D_{2h} and $b_g + b_u$ in C_{2h}. [c] Recall that the orbital sequence in the 4+ species, is reversed from that in the 3+ and 2+ species. π^* label sequence as in free bridge ligand.

4−9). The INDO model, as available in the ZINDO program (see the Experimental Section), has proven very useful in reproducing the electronic spectra and structure of ruthenium(II) complexes.[9,64−70] As a check, we have also compared the results of density functional theory (DFT) calculations for the archetypal $[Ru(bpy)_3]^{2+}$ ion[71] with our ZINDO analysis, with very similar results with respect to predictions of transition energies and the degree of mixing between metal and ligand orbitals. Extended Hückel calculations[13c] on the group of complexes discussed here also give generally similar results with respect to orbital mixing.

The electronic structures and predicted spectra of the C_{2h} and D_2 stereoisomers are similar, and the available electronic spectra do not permit them to be distinguished. Indeed Keene and coworkers[59a] reported electronic spectroscopic data for separated pairs of similarly bridged diastereoisomers. The spectra are closely similar in appearance with little change in relative intensities and only small shifts in band energies. We therefore exclusively consider the C_{2h} stereoisomer in the remainder of the paper.

The quality of the INDO/S calculations was assessed by comparing the ZINDO/S-derived electronic spectra of the various members of the redox series to the experimental spectra (Figure 3). Reasonable agreement between experimental and predicted spectra using Hartree−Fock theory was observed for all three species, with assignments consistent with general expectation based on previous experience. We therefore have confidence in the conclusions that can be reached using the INDO model in analyzing these ruthenium systems.

C.6.1. Free Ligand 1,2,4,5-Tetraimino-3,6-diketocyclohexane Molecular Orbital Diagram. Figure 4a shows an MO diagram for the bridging ligand using the same nuclear coordinates as employed in the ZINDO/1-optimized structure of **2**, while Figure 4b displays a selection of key frontier orbitals. The bridging ligand has local D_{2h} symmetry, and we utilize a coordinate framework for the free ligand and complexes in which the Ru−Ru vector lies along *y* and the bridge lies in the *xy* plane; *z* is the bridge perpendicular. The free ligand has three relatively low lying π^*-orbitals labeled b_{1u} ($\pi^*(1)$), b_{2g} ($\pi^*(2)$), and b_{3g} ($\pi^*(3)$) (Figure 4b). These lie below the π^*-bipyridine orbitals in the complexes and are empty in species **2**. Two of these three orbitals, b_{1u} and b_{3g}, provide the dominant pathway for coupling the two metal centers. The HOMO of the free ligand (Figure 4a) is a σ-orbital (b_{2u} symmetry), but it will drop in energy when the ligand coordinates to the Ru(II) center. HOMO − 1 of b_{2g} symmetry and HOMO − 3 of a_u symmetry also provide a coupling pathway (see below).

C.6.2. A ZINDO Molecular Orbital Analysis of Complexes 2, 3, and 4. The filled ruthenium 4d-orbitals (Ru(II), d^6), which in a standard octahedron would be the π t_{2g} orbitals, comprise in D_{2h} symmetry, with respect to the bridging ligand, the π-(d_{yz})-, δ(d_{xz})-, and σ($d_{x^2-y^2}$)-orbitals. These orbitals combine in- and out-of-phase across the bridging ligand, generating the symmetry-adapted metal combinations (SAMC) with the symmetries in Table 7, shown with respect to both the D_{2h} symmetry of the bridging ligand and the C_{2h} symmetry of the entire molecule. We shall discuss the bonding in terms of local D_{2h} symmetry, since this makes the assessment much clearer.

The in- and out-of-phase coupling of the metal d_{yz}-orbitals $\{d_{yz}(1) \pm d_{yz}(2)\}$ (written below in short form $d\pi^{\pm}$) permits them to overlap the b_{1u} and b_{3g} π^*(bridge)-orbitals. The metal $d_{x^2-y^2}$ orbitals lie in the bridge molecular plane and can only be coupled through bridging ligand σ-orbitals. There is both a low-lying π^*-orbital (LUMO + 1) and a filled π-orbital (HOMO − 1) of b_{2g} symmetry that may couple with the in-phase $\delta(d_{xz})$ combination, while the out-of-phase $\delta(d_{xz})$ combination requires an a_u π^*-orbital that lies at much higher energy. Free ligand HOMO − 3 is also a_u (Figure 4b).

A primary interest in analyzing these data is to assess the extent of coupling across the bridge, i.e., to identify the extent to which the ruthenium d-orbitals on either side of the bridge communicate. This may be appreciated by the degree of mixing between metal d-orbitals and ligand π- and π^*-orbitals, and also by the magnitude of the splitting between the in- and out-of-phase pairs above. To first order, if the ruthenium atoms on either side of the bridge do not "sense" each other, the splitting would be zero. The mechanism for sensing each other is for each metal SAMC to couple through a bridge orbital of the same symmetry as the SAMC. For example, it is differential combination with ligand b_{1u} and b_{3g} orbitals which provides the mechanism to split the $d_{yz} \pm d_{yz}$ levels.

The most significant Ru-d/bridging ligand overlap is expected between the bridging ligand π^* b_{1u} and π^* b_{3g} orbitals and the $d\pi^{\pm}$ SAMCs. Net overlap between the bridge ligand π^* b_{2g} and Ru $d\delta^+$ is likely to be much less important. However, as noted, there will also be overlap with filled π-orbitals of the bridge ligand of appropriate symmetry. The net splitting between the pairs of SAMCs may be the best indicator of "information transfer".

This is a rather oversimplified picture, since the 2,2′-bipyridine ligands reduce the effective symmetry of this complex to C_{2h}. In D_{2h} symmetry all six combinations of the pair of 4d-(t_{2g}) orbitals on each Ru center transform as a different

(64) Broo, A.; Lincoln, P. *Inorg. Chem.* **1997**, *36*, 2544.
(65) McDonagh, A. M.; Whittall, I. R.; Humphrey, M. G.; Hockless, D. C. R.; Skelton, B. W.; White, A. H. *J. Organomet. Chem.* **1996**, *523*, 33.
(66) McDonagh, A. M.; Whittall, I. R.; Humphrey, M. G.; Skelton, B. W.; White, A. H. *J. Organomet. Chem.* **1996**, *519*, 229.
(67) Shin, Y.-G.; Brunschwig, B. S.; Creutz, C.; Sutin, N. *J. Phys. Chem.* **1996**, *100*, 8157.
(68) Shin, Y. K.; Brunschwig, B. S.; Creutz, C.; Newton, M. D.; Sutin, N. *J. Phys. Chem.* **1996**, *100*, 1104.
(69) Shin, Y.; Brunsschwig, B. S.; Creutz, C.; Sutin, N. *J. Am. Chem. Soc.* **1995**, *117*, 8668.
(70) Gorelsky, S. I.; Dodsworth, E. S.; Vlcek, A. A.; Lever, A. B. P. *Coord. Chem. Rev.* **1998**, *174*, 469.
(71) Daul, C.; Baerends, E. J.; Vernooijs, P. *Inorg. Chem.* **1994**, *33*, 3538

Table 6. Sums of Molecular Orbital Coefficients and Overall d Splitting Energies

	MOs 147−152			d_{yz} combinations[b]		overall d	overall bpy $\pi^*(1)$
	Ru d[a]	bridge	bpy	Ru d_{yz} b_{1u}	Ru d_{yz} b_{3g}	splitting,[c] cm^{-1}	splitting,[d] cm^{-1}
4+	3.66 (4.3)	0.82	1.53	0.28	0.52	3220	220
3+	3.78 (4.10)	0.65	1.57	0.48	0.59	3550	220
2+	3.90 (4.17)	0.81	1.30	0.53	0.63	4520	470

[a] Sum over nos. 147−155. [b] Maximum would be 1. [c] Orbitals 147−152. [d] Energy difference between the first and second pairs of bpy π^* levels.

Table 7. ZINDO/S Frontier Orbital Energies, Symmetries and Fractional Contributions for the 4+ Species [Data Rounded to Two Decimal Places][a,b]

orbital	energy	total Ru	bpy	bridge	$\Gamma(D_{2h})$	$\Gamma(C_{2h})$
142	−18.92	0.00	0.98	0.02		
143	−17.33	0.07	0.92	0.01	b_{2g}, $d\delta^+$	a_g
144	−17.32	0.13	0.74	0.13	b_{1u}, $d\pi^-$	b_u
145	−17.32	0.06	0.93	0.01	a_u, $d\delta^-$	a_u
146	−17.27	0.03	0.95	0.02	b_{3g}, $d\pi^+$	b_g
147	−17.04	0.28	0.41	0.31	b_{1u}, $d\pi^-$	b_u
148	−16.82	0.73	0.19	0.08	b_{2g}, $d\delta^+$	a_g
149	−16.75	0.76	0.17	0.07	a_u, $d\delta^-$	a_u
150	−16.66	0.68	0.29	0.02	a_g, $d\sigma^+$	a_g
151	−16.64	0.52	0.18	0.30	b_{3g}, $d\pi^+$	b_g
152 H	−16.64	0.69	0.28	0.03	b_{2u}, $d\sigma^-$	a_u
153 L	−11.73	0.37	0.06	0.57	b_{1u}, $d\pi^-$	b_u
154	−11.06	0.03	0.00	0.97	b_{2g}, $d\delta^+$	a_g
155	−10.99	0.25	0.06	0.69	b_{3g}, $d\pi^+$	b_g
156	−9.71	0.03	0.96	0.01	b_{1u}, $d\pi^-$	b_u
157	−9.71	0.04	0.95	0.01	b_{3g}, $d\pi^+$	b_g
158	−9.68	0.03	0.97	0.00	b_{2u}, $d\sigma^-$	a_u
159	−9.68	0.03	0.97	0.00	a_g, $d\sigma^+$	a_g
160	−8.81	0.01	0.99	0.00		

[a] H = HOMO. [b] Data for ruthenium include 4d, 5s, and 5p contributions, but those for 5s and 5p are extremely small. Thus, the total sum should be 1.00. Deviations of ±0.01 are due to round-off errors.

Table 8. ZINDO/S Frontier Orbital Energies and Fractional Contributions for the 3+ Species[a]

orbital	energy, eV	total Ru	bpy	bridge	$\Gamma(D_{4h})$	$\Gamma(C_{2h})$
142	−16.39	0.00	0.05	0.94		
143	−15.19	0.04	0.95	0.01	a_g, $d\sigma^+$	a_g
144	−15.19	0.04	0.96	0.01	b_{2u}, $d\sigma^-$	a_u
145	−15.16	0.07	0.90	0.03	b_{1u}, $d\pi^-$	a_u
146	−15.14	0.04	0.95	0.01	b_{3g}, $d\pi^+$	b_g
147	−14.72	0.48	0.31	0.21	b_{1u}, $d\pi^-$	a_u
148	−14.52	0.59	0.25	0.16	b_{3g}, $d\pi^+$	b_g
149	−14.50	0.70	0.20	0.10	b_{2g}, $d\delta^+$	a_g
150	−14.45	0.71	0.20	0.10	a_u, $d\delta^-$	a_u
151	−14.32	0.65	0.32	0.04	a_g, $d\sigma^+$	a_g
152	−14.28	0.66	0.30	0.04	b_{2u}, $d\sigma^-$	a_u
153 S	−12.81	0.18	0.03	0.79	b_{1u}, $d\pi^-$	b_u
154 S[b]	−12.24	0.12	0.02	0.86	b_{3g}, $d\pi^+$	b_g
155	−11.77	0.02	0.00	0.98	b_{2g}, $d\delta^+$	a_g
156	−10.09	0.01	0.01	0.98	a_u, $d\delta^-$	a_u
157	−9.90	0.03	0.96	0.01		
158	−9.89	0.03	0.97	0.00		
159	−9.87	0.04	0.96	0.00		
160	−9.86	0.04	0.95	0.01		

[a] See footnotes to Table 7. S = SOMO. [b] See the text regarding CAHF.

representation. The in- and out-of-phase combinations of the dσ*-orbitals (d_{z^2} and d_{xy} in this framework) transform as (a_g + b_{2u}) and (b_{1g} + b_{3u}), respectively, in D_{2h}, and these representations do not occur within the set of six 4d(t_{2g}) representations (see Tables 5 and 6). However, in C_{2h} symmetry, where the *y* axis in D_{2h} becomes the *z* axis, all the d(t_{2g}) combinations can couple to a dσ* combination of appropriate symmetry (see Table 5 and its footnotes).

Table 9. ZINDO/S Frontier Orbital Energies, Symmetries and Fractional Contributions for the 2+ Species[a]

MO index	energy, eV	total Ru	bpy	bridge	$\Gamma(D_{2h})$	$\Gamma(C_{2h})$
142	−13.34	0.01	0.02	0.97		
143	−12.98	0.02	0.97	0.01		
144	−12.98	0.02	0.97	0.01		
145	−12.94	0.02	0.97	0.01		
146	−12.94	0.01	0.98	0.00		
147	−12.17	0.53	0.22	0.25	b_{1u}, $d\pi^-$	b_u
148	−11.92	0.63	0.21	0.16	b_{3g}, $d\pi^+$	b_g
149	−11.74	0.67	0.23	0.10	b_{2g}, $d\delta^+$	a_g
150	−11.69	0.66	0.25	0.08	a_u, $d\delta^-$	a_u
151	−11.67	0.70	0.21	0.10	a_g, $d\sigma^+$	a_g
152	−11.61	0.71	0.17	0.12	b_{2u}, $d\sigma^-$	a_u
153 H[b]	−10.06	0.17	0.04	0.79	b_{1u}, $d\pi^-$	b_u
154 H[b]	−9.495	0.08	0.03	0.89	b_{3g}, $d\pi^+$	b_g
155 L[b]	−7.49	0.01	0.00	0.98	b_{2g}, $d\delta^+$	b_g
156	−6.815	0.03	0.96	0.01		
157	−6.81	0.03	0.96	0.01		
158	−6.75	0.05	0.94	0.01		
159	−6.75	0.05	0.94	0.01		
160	−5.96	0.02	0.98	0.00		

[a] See footnotes to Table 7. [b] See the text regarding CAHF.

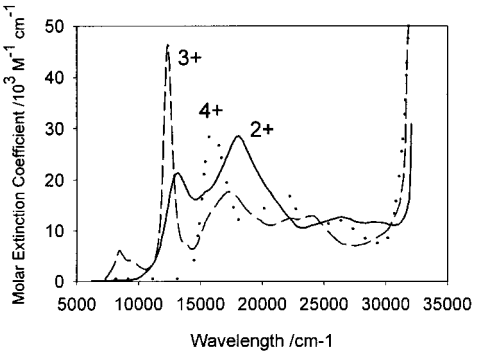

Figure 3. Electronic spectra of [{Ru(bpy)$_2$}$_2$(tetraiminodiketocyclohexane)]$^{n+}$ species **2**−**4** (6.24×10^{-5} M), obtained spectroelectrochemically in CH_3CN containing 0.3 M Bu_4NPF_6. Solid line: $n = 2$, $E = -0.27$ V. Short-dashed line: $n = 3$, $E = 0.1$ V. Long-dashed line: $n = 4$, $E = 0.55$ V (potentials vs SCE).

The theoretical spectrum of **2** was calculated several times using the ZINDO/S routine in Hyperchem, first using nuclear coordinates obtained from X-ray crystallography, then using nuclear coordinates obtained by ZINDO/1 geometry optimizations, and, finally, changing the π-overlap weighting factor from 0.585 to 0.640. The ZINDO/1-optimized structure gave slightly better agreement with experiment, and for consistency, we have chosen to use ZINDO/1-optimized structures to calculate the entire redox series. The π-overlap weighting factor significantly affects the energies and oscillator strengths of the predicted spectra. Generally, the transition energies and intensities increase when using a larger factor. The standard value of 0.585 was adopted. The key bond distances employed (Table 10) agree overall with the crystal structure reported here and with relevant bipyridine ruthenium species in the literature.

For the open shell 3+ species (**3**) we have used both ROHF (restricted open shell Hartree−Fock) and CAHF (configuration-

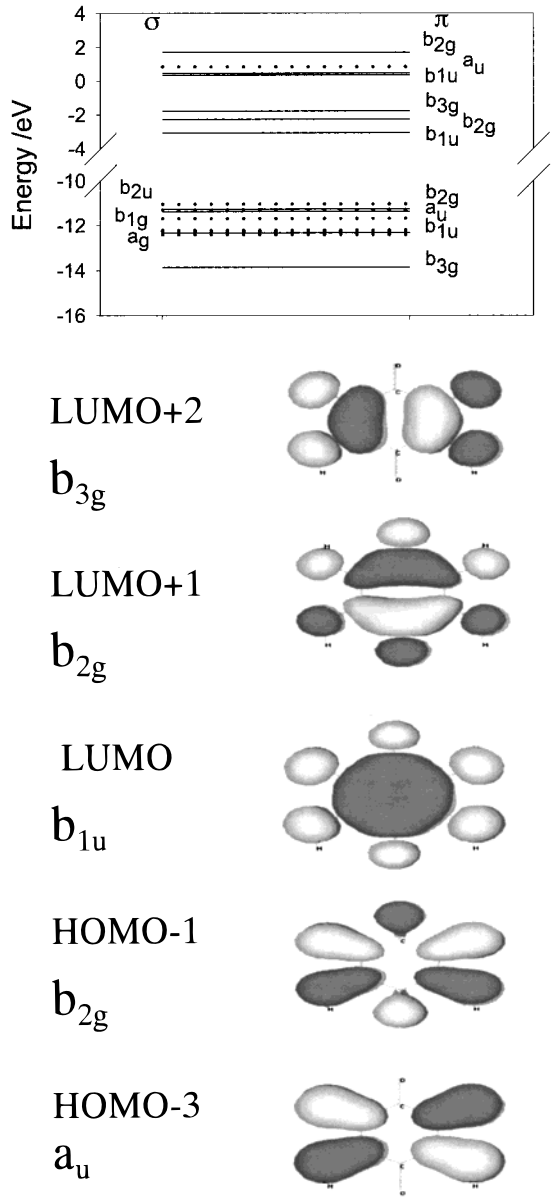

Figure 4. (a, top) A MO diagram for the uncomplexed 1,2,4,5-tetraimino-3,6-diketocyclohexane bridging ligand, derived from INDO/S and the INDO/1 geometry-optimized-structure of [{Ru(bpy)$_2$}$_2$-(tetraiminodiketocyclohexane)]. The solid lines are π levels as identified by their symmetry labels. The hatched lines are σ levels. The HOMO is a σ level, b_{2u}, but this will be stabilized below the π levels upon complexation to ruthenium. Not all the σ levels are identified in this diagram. (b, bottom) Examples of the frontier molecular orbitals of the free bridging ligand as defined in (a).

Table 10. Principal Bond Distances Used in ZINDO/S Calculations (Å) and Calculated Using ZINDO/1-Based Geometry Optimization for the [{Ru(bpy)$_2$}$_2$(tetraiminodiketocyclohexane)]$^{n+}$ Binuclear Complexes

	4+	3+	2+
Ru−N(bpy)	2.0499	2.0495	2.037
Ru−NH(bridge)	2.049	2.052	2.034
C═NH (bridge)	1.3199	1.334	1.346
C═O (bridge)	1.279	1.2896	1.297

averaged Hartree−Fock).[41] In the former case the calculation leads to a split symmetry solution, suggesting some asymmetric $Ru^{III}-L^{2-}-Ru^{II}$ valence bond configuration mixed with the symmetric $Ru^{II}-L^{1-}-Ru^{II}$ situation. Such broken symmetry solutions are common when the interaction between the two metals is weak.[42] Configuration interaction of sufficient size would add back the other component of the split symmetry solution, $Ru^{II}-L^{2-}-Ru^{III}$, again yielding a symmetric solution. The interaction between these two valence configurations $Ru^{III}-L^{2-}-Ru^{II}$ and $Ru^{II}-L^{2-}-Ru^{III}$ is supposedly small, and would not change the general overall features of the results, provided the nuclear symmetry of the system is not reduced to reinforce the split symmetry.

Table 11. Comparison of ROHF and CAHF Solutions to the Electronic Structure of **3**

energy (hartrees)	SCF	+CI
CAHF	−457.695 71	−457.709 49
ROHF	−457.709 81	−457.711 55
difference	0.0141	0.0021

	SCF		+CI	
Mulliken population, e$^-$	Ru1	Ru2	Ru1	Ru2
CAHF	7.12	7.12	7.11	7.11
ROHF	7.09	7.15	7.11	7.14

The CAHF scheme[41] assigns one electron to each of the two low-lying π^* orbitals on the bridge and averages over these two configurations. This restores the symmetry as anticipated. The SCF results are of higher energy than obtained from the ROHF doublet state, as expected, but only by 0.0141 hartree (8.8 kcal/mol).

After configurational interaction (CI) the two solutions differ only by 0.0021 hartree (1.3 kcal/mol), as seen in Table 11. The broken symmetry solution is still of lower energy, but both calculations will lead to the same symmetric result if a large enough CI could be performed on both. It is clear from this analysis, however, that the mixed valence bond configuration is part of the ground-state description.

The low-energy transitions calculated for the 3+ ion appear to be calculated somewhat more accurately from the lower energy ROHF split symmetry reference state, but the symmetric case is far easier to interpret and to relate to the 2+ and 4+ ions.

A RHF calculation of the 2+ species, **4**, led to the lowest lying spin triplet state to have a negative energy (relative to the ground state); i.e., the calculation predicts that the $S = 1$ ground state lies slightly below the $S = 0$ ground state; experimentally this is not the case. However, if it is assumed, as with the open shell species **3**, that the next π^* state on the bridge is partially occupied and one carries out a CAHF analysis over the configurations $|1\alpha1\beta...152\alpha152\beta153\alpha153\beta|$ and $|1\alpha1\beta...152\alpha152\beta154\alpha154\beta|$, then the $S = 0$ state is predicted to lie below the $|1\alpha1\beta...152\alpha152\beta153\alpha154\alpha|$ $S = 1$ state, where $|...|$ is the usual Slater determinant.

There is a general increase in the MO energies of roughly 2.2 eV accompanying each electron added to the binuclear complex, simply due to increased electrostatic repulsions. We have compensated for this effect in Figure 5 by normalizing the MO energies of the three redox species to the highest filled π(bpy) [no. 146] level. From our past experience with Ru(bpy)$_2$LL complexes, where LL is an electroactive ligand, the π and π^*(bpy)-orbitals do not couple appreciably with those of LL, and changes in their energy, due to the reduction of LL, reflect the general electrostatic repulsions felt by all of the orbitals. Indeed, in the binuclear redox series, the lowest lying π^*-orbitals on each of the four bipyridine units couple so weakly across the bridge that they create four, nearly degenerate, π^*-(bpy)-MOs (separation ca. 220−470 cm^{-1}; see Table 6). This is apparently also true for the filled bipyridine π-orbitals (and the π^*(2) bpy orbitals).

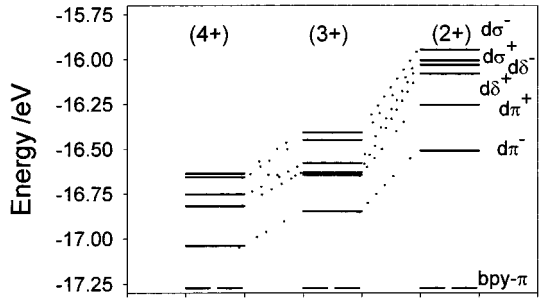

Figure 5. Energy level diagrams showing how the $d(t_{2g})^{\pm}$-orbitals of the $[\{Ru(bpy)_2\}_2(tetraiminodiketocyclohexane)]^{n+}$ binuclear species change as a function of oxidation state. The energy levels are normalized to the π bpy level no. 146 as zero to provide a common internal reference.

Using the so-called "dimer splitting" method,[72] simplifying the coupling to a pair of d-orbitals mediated by the bridge and excluding mixing with other orbitals (i.e., assuming D_{2h} symmetry), the energy separation between the in- and out-of-phase combinations of the d-orbital pair is equal to $2H_{ab}$, where H_{ab} is the electronic matrix coupling element. These data are shown in Table 5. Coupling (H_{ab}) through the *yz* pathway appears to vary from (2) 1610 cm^{-1} to (**3**) 805 cm^{-1} to (**4**) 1005 cm^{-1} but remains less than that observed (3140 cm^{-1}) in the Creutz−Taube complex.[26] The H_{ab} values are however appreciably larger than observed in most other bridged species.[26] Coupling through the Ru dδ pathway is substantially smaller while that for the σ pathway[73] is very small (Table 5) for 2 and 3 but somewhat greater for 4 due to the extra negative charge on the bridge.

Consistent with the substantial splitting of the *yz* combinations, the b_{1u} MO ($d\pi^-$, no. 147 in all three species) possesses the smallest ruthenium content, i.e., is most mixed with ligand orbitals, both bridge and bpy (Figure 6, Tables 5−9), and is the most stabilized of the $d(t_{2g})^{\pm}$ set. Data collected in Table 6 illustrate that the overall mixing between $d\pi^+$ and $d\pi^-$ with the ligands decreases from the 4+ to the 3+ to the 2+ species due surely to the increasing formal negative charge on the bridge.

In species 2, the ruthenium content of the b_{1u} π^*-orbital [no. 153] and b_{3g} orbital [no. 155] is substantial, being about 36% and 25%, respectively (Tables 5 and 7). From this, we can deduce that π-back-donation has resulted in a net transfer of about 0.7 e^- to b_{1u} and 0.5 e^- to b_{3g}, or a total transfer of over 1 e^- to the bridge. Back-donation into the π^* bridge orbitals remains substantial upon reduction. The LUMO of species **2** [no. 153] is filled in 4. While it is still an antibonding bridge π^*-orbital, it has very substantial Ru content (17%, Tables 5 and 9). However, overall back-donation to the bridge does decrease from the 4+ to the 3+ to the 2+ species (Table 5) for the reason noted above. We caution however that the reliability of the derived MO coefficients for the virtual orbitals is lower than for the filled orbitals.

The d_{xz} $d\delta^{\pm}$ combination splits to a much smaller degree than $d\pi^{\pm}$ (Table 5), and the ruthenium content of these levels is much higher; i.e., there is less mixing with the ligand due to poor net overlap. This is also reflected in the fact that the ligand π^* b_{2g} orbital has very little ruthenium content.

The $d_{x^2-y^2}$ $d\sigma^{\pm}$ combination splits hardly at all in the 2+ and 3+ species, indicating very poor coupling through the σ-manifold of the bridge. It is somewhat larger in the 2+ species (Table 5) (see below).

(72) Joachim, C.; Launay, J. P.; Woitellier, S. *Chem. Phys.* **1990**, *147*, 131.
(73) Escuer, A.; Vicente, R.; Mernari, B.; El Gueddi, A.; Pierrot, M. *Inorg. Chem.* **1997**, *36*, 2511.

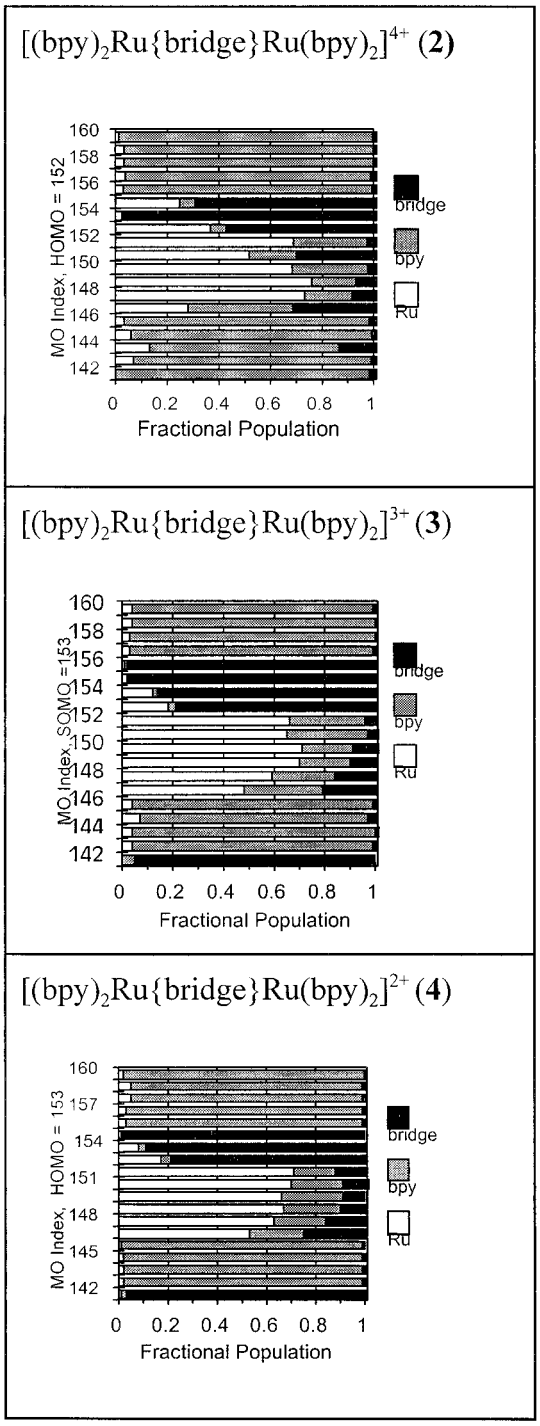

Figure 6. Diagram showing the fractional contribution of total Ru (white) (equal contributions from each Ru), bridge (black), and bipyridine (gray) character in the $d(t_{2g})^{\pm}$ orbitals of species **2**, **3**, and **4**. A color version can be seen for these species at http://www.chem.yorku.ca/profs/lever/blever.htm.

The sequence of d-orbitals is determined by a complex interplay of destabilization from filled frontier ligand levels,[9] and stabilization by interaction (back-donation) with the empty π^* levels. The $d\pi^-$ b_{1u} level is always well stabilized, while the $d\sigma^-$ b_{2u} is always destabilized. Indeed, Figure 5 shows that the sequence of d-orbitals is the same for all three systems except for the unusual destabilization of $d\pi^+$ in the 4+ ion.

A parallel procedure to assess the extent of mixing is to sum the total ruthenium and bridge and bipyridine contributions to the six t_{2g} orbitals as a function of oxidation state. This is

summarized in Table 6. If there were no mixing between metal and ligand orbitals, the sum over MOs 147−152 (the t_{2g} set in each Ru) would be six for the Ru d set and zero for the bridge and bipyridine orbitals. The nonzero values for the bridge and bpy orbitals over this set is a qualitative indicator of the extent of mixing among metal, bridge, and bipyridine MOs. The variation in bpy and bridge contribution is not great, but the smaller contribution for bpy in **4** may reflect a decrease in mixing between filled metal and filled bpy π-orbitals (which lie close to the d(t_{2g}) set, Tables 7−9) due to the decreased Lewis acidity of the Ru^{II} center in this species. This decrease is seen in Figure 5 where the Ru d levels rise in energy appreciably and can also be seen experimentally from the Ru d → bpy (π*) transitions (Table 4) which are significantly red shifted in the 2+ species relative to where they are observed in the 3+ and 4+ species. The sharp reduction in the bridge contribution for species **3** in MOs 147−152 relative to **2** and **4** is likely due to the fact that the latter two species contain a quinonediimine acceptor fragment while **3** has more semiquinonediimine character.

There is also a greater splitting of the π*(1) bpy manifold (Table 5) indicative of somewhat enhanced back-donation to the π*(1) bpy levels, causing some differential destabilization.[70] The actual amount of back-donation is very small but does appear greater for the 2+ species than for 3+ and 4+ (Tables 7−9) due to greater negative charge on the ruthenium centers.

Finally we note that the overall splitting of the d(t_{2g})$^{\pm}$ set is substantially greater for the 2+ ion than for the 4+ ion (Tables 5 and 6). Close scrutiny of Figure 5 reveals that this is due to a greater σ* destabilization of the dσ^- and dσ^+ levels by the more electron rich and σ-donating doubly reduced bridging ligand rather than stabilization of the dπ^+ and dπ^- levels.

C.6.3. Electronic Spectra. C.6.3.1. The 4+ Binuclear (Ru^{II}−(L)−Ru^{II})$^{4+}$, 2 {Electronic Configuration...[No. 152]^2}. In the following discussions, names such as d → π*(bridge) will generally be used for assigning transitions to the three low-lying π*(bridge)-orbitals, while a more detailed assignment, in terms of symmetry labels and orbital numbering, can be found in Table 4.

Configurational interaction (CI) involving the top 18 filled and the lowest 18 empty orbitals (648 single excited-state configurations, CIS) were used to calculate the electronic spectra. The use of a larger CI basis had little impact on the predicted energies. We are mainly interested in metal to ligand charge-transfer (MLCT) transitions[74] to the bridging ligand.

In simple mononuclear ruthenium benzoquinone systems, the most intense MLCT-type transition is expected to be between the MOs generated through mixing between the π-back-donating d-orbital and the π-acceptor LUMO ligand orbital.[2,3,5,7,9,74] By analogy, the most intense MLCT to bridge transition in species **2** should be from the b_{3g} dπ^+ SAMC [no. 151] to the b_{1u} π*-(bridge) − dπ^- LUMO [no. 153], and this is, indeed, predicted to be the lowest lying intense transition in the spectrum (Table 4). This can be described as a mixed dπ^+ → dπ^- transition, and one or more of these transitions can expected to be strong and observed in all three complexes, terminating on π*(bridge)−dπ^+ or π*(bridge) − dπ^-. Similarly, d$\delta^{\pm}$ → d$\delta^{\pm}$ types of transitions can be expected to be fairly strong and are observed.

Indeed, the next major feature (21 350 cm^{-1}) is the dδ^- → π*(bridge) − dδ^+ (b_{2g}) transition, apparently mixed with some π(bpy) → π*(bridge) component. Following this (Table 4) is a broad absorption region clearly encompassing many bands including the other "d_{yz}" transition, from the deeper lying b_{1u} dπ^- SAMC [no. 147] to the b_{3g} π*(bridge) − dπ^+ [no. 154] and from about 28 000 cm^{-1} to d → π*(bpy).

C.6.3.2. The 3+ Binuclear (Ru^{II}−(L^-)−Ru^{II})$^{3+}$, 3 {Electronic Configuration...[No. 152]^2[No. 153]^1 Mixed with ...[No. 152]^2[No. 154]^1}. When species **2** is reduced, an electron is introduced into the b_{1u}, π*(bridge) LUMO [no. 153]; the orbital then becomes a singly occupied MO (SOMO). As noted above, there is also a contribution from partial occupation of orbital no. 154. Several low-energy transitions can be expected, specifically SOMO [no. 153] → LUMO [no. 154] and SOMO → LUMO + 1 [no. 155]. These are symmetry-allowed u→ g transitions, and are assigned to the weak near-IR absorption. The INDO/S calculation predicts such low-energy near-IR transitions though at rather lower energy than observed experimentally. The very narrow and intense band at 12 350 cm^{-1} must involve a transition between mixed states[74] of similar geometry and is therefore surely assigned to the dπ^+ b_{3g} → π*(bridge) − dπ^- b_{1u} transition. Indeed ZINDO/S predicts this band at 11 350 cm^{-1} assigned as [no. 148 → no. 153], which is the aforementioned transition.

Experimentally, there follow a series of overlapping relatively weak transitions, and ZINDO/S assigns these to additional d → π*(bridge) transitions and to d → π* (bpy) transitions. The latter are found at lower energy than in the 4+ species. Agreement between experimental and predicted spectra is quite reasonable.

C.6.3.3. The 2+ Binuclear (Ru^{II}−(L^{2-})−Ru^{II})$^{2+}$, 4 {Electronic Configuration...[No. 153]^2 Mixed With ...[No. 154]^2}. It is reasonable as with species **3** to assign the lowest transition as an internal bridge transition from no. 153 to no. 154, no. 155, and the calculation confirms this. Since the ligand b_{1u} orbital [no. 153] is now full and the ligand has formal 2− charge, there will be no low-lying d → π*(bridge) MLCT bands. Indeed INDO/S predicts the next group of transitions to be solely d → π*(bpy) in nature. The dπ^- → dπ^+ type transitions being excitations from no. 147 and no. 148 to no. 154 and no. 153, respectively, at ca. 28 000 cm^{-1}, are the lowest lying predicted M → bridge MLCT bands in this species. Overall agreement between predicted and observed transitions (Table 4) is good.

C.6.3.4. Spectroscopic Trends across the Series. From Figure 5, it is clear that the "t_{2g}" orbitals generally increase in energy with respect to the π*(bpy) levels (due to charge transferred from the reduced bridge ligand to ruthenium), and this is reflected in the experimentally observed red shift of d → π*(1)(bpy) bands as the binuclear complex is reduced. The low-lying dπ^+ → dπ^- transition in **2** arises because of the significant destabilization of the donor dπ^+ [no. 151] orbital in **2**. The dπ^+ → dπ^- type transitions then shift to higher energy in **3** and then **4** as the charge on the bridge increases.

D. Concluding Remarks. A primary objective of this research is to assess the extent of coupling through the bridge as exemplified by the magnitudes of the H_{ab} electronic coupling matrix elements considered proportional to the splitting between in- and out-of-phase coupled pairs of d-orbitals. As discussed above, these can be extracted in terms of the symmetry of the pathway involved, and the magnitudes generally follow the sequence d$\pi^{\pm}$ > d$\delta^{\pm}$ > d$\sigma^{\pm}$. However, because of the enhanced basicity of the doubly reduced bridge, the d$\sigma^{\pm}$ splitting in **4** is comparable to the d$\delta^{\pm}$ splitting. Because the true symmetry is C_{2h} rather than D_{2h}, the splitting energies are actually a more complex function of the electronic coupling but nevertheless should be an adequate estimate of the extent of coupling across the bridge.

(74) Lever, A. B. P. *Inorganic Electronic Spectroscopy*; Elsevier Science Publishers: New York, 1984.

The combined ZINDO and spectroelectrochemical study reveals a system with very strong coupling across the bridging ligand. This is especially true of the 4+ species where the primarily bridge ligand based LUMO and LUMO + 2 formally have a total of 37% and 25% contribution from the metal. The ZINDO calculations have provided a good deal of insight into the electronic behavior of these complexes, and we are confident that the analysis is basically correct. The extent of mixing is substantial, being further evidence for the close match in orbital energies and good overlap in ruthenium quinonoid systems.[2,6,7,9,11,14,70,75,76] Mixing increases as the bridge is reduced due to a synergistic interaction whereby the ruthenium centers become more polarizable and return electron density to the bridge. Both ligand π and π^* levels are clearly involved.

(75) Lever, A. B. P.; Masui, H.; Metcalfe, R. A.; Stufkens, D. J.; Dodsworth, E. S.; Auburn, P. R. *Coord. Chem. Rev.* **1993**, *125*, 317.
(76) da Cunha, C. J.; Dodsworth, E. S.; Monteiro, M. A.; Lever, A. B. P. *Inorg Chem.* **1999**, *38*, 5399.

Acknowledgment. We thank Drs. Elaine S. Dodsworth and Pamela R. Auburn for useful discussions, Johnson Matthey for the loan of ruthenium trichloride, and the Natural Sciences and Engineering Research Council (NSERC, Ottawa) for financial support. Calculations were supported in part by a SUR grant from IBM.

Supporting Information Available: Figure S1 showing the EPR spectrum of $[\{Ru(bpy)_2\}_2(tetraiminodiketocyclohexane)](PF_6)_3$ and Table S1 giving principal bond distances used in ZINDO/S calculations and calculated using ZINDO/1-based geometry optimizations for the $[\{Ru(bpy)_2\}_2(tetraiminodiketocyclohexane)]^{n+}$ binuclear complexes. This material is available free of charge via the Internet at http://pubs.acs.org. This information, together with color versions of Figure 6 for all three species, and examples of some of the molecular orbitals can also be found at http://www.chem.yorku.ca/profs/lever/blever.htm following the links to this publication.

IC980826Q